Chemistry–A European Journal
Research Article
doi.org/10.1002/chem.202203584
Chemistry Europe
European Chemical Societies Publishing
www.chemeurj.org

Widening the Landscape of Small Molecule Activation with Gold-Aluminyl Complexes: A Systematic Study of E–H (E = O, N) Bonds, SO_2 and N_2O Activation

Diego Sorbelli,*[a, b] Leonardo Belpassi,*[b] and Paola Belanzoni*[a, b]

Abstract: The electronic features of gold-aluminyl complexes have been thoroughly explored. Their similarity with Group 14 dimetallenes and other metal-aluminyl complexes suggests that their reactivity with small molecules beyond carbon dioxide could be accessed. In this work, the reactivity of the [^{t}Bu$_3$PAuAl(NON)] (NON = 4,5-bis(2,6 diisopropylanilido)-2,7-ditert-butyl-9,9-dimethylxanthene) complex towards water, ammonia, sulfur dioxide and nitrous oxide is computationally explored. The reaction mechanisms computed for each substrate strongly suggest that all activation processes are in principle experimentally feasible. Electronic structure analysis highlights that, in all cases, the reactivity is driven by the presence of the poorly polarized electron-sharing gold-aluminyl bond, which induces a radical-like reactivity of the complex towards all the substrates. A flat topology of the potential energy surface (PES) has been found for the reaction with N_2O, where two almost isoenergetic transition states can be located along the same reaction coordinate with different geometries, suggesting that the N_2O binding mode may not be a good indicator of the nature of N_2O activation in a cooperative bimetallic reactivity. In addition, the catalytic potentialities of these complexes have been explored in the framework of nitrous oxide reduction. The study reveals that the [^{t}Bu$_3$PAuAl(NON)] complex might be an efficient catalyst towards oxidation of phosphines (and boranes) via N_2O reduction. These findings underline recurring trends in the novel chemistry of gold-aluminyl complexes and call for experimental feedbacks.

Introduction

Recently, an experimental work has been reported describing the unique reactivity of the gold-aluminyl complex **1** (see Scheme 1) with carbon dioxide, yielding the CO_2 insertion product **2**.[1] The Au–C coordination mode in **2** led to suggest the presence of an unprecedented nucleophilic gold site in the complex.[1] Several works by us have followed, where, by combining mechanistic studies and extensive electronic structure analysis, we demonstrated that this unusual reactivity is actually a cooperative radical-like reactivity induced by the presence of an electron-sharing poorly polarized Au–Al bond in **1**.[2–7]

Consistently with the small degree of polarization of the Au–Al bond in **1**, this reactivity is very similar to the reactivity of Group 14 dimetallenes and dimetallynes[8] such as digermylene compounds **3**, which have been reported, driven by the covalent non-polarized Ge–Ge bond, to insert CO_2 (**4**) within a very similar fashion with respect to **1**.[9] Furthermore, this class of compounds has been shown to efficiently activate other substrates by relying on these electron-sharing E–E (E = Si, Ge, Sn) bonds.[8] For instance, digermylenes have been shown to activate dihydrogen in relatively mild experimental conditions via the formation of the singly-bridged [RGe(μ-*H*)Ge(H)(R)] intermediate (**5**).[10–13] Inspired by this evidence and by the strict analogy between Ge–Ge and Au–Al bonds, we very recently reported that analogous H_2 activation by **1** via formation of the singly-bridged [^{t}Bu$_3$PAu(μ-*H*)Al(H)(NON)] (NON = 4,5-bis(2,6 diisopropylanilido)-2,7-ditert-butyl-9,9-dimethylxanthene) species is in principle feasible and ideal for the use of **1** as hydrogenation catalyst.[14]

Analogies between coinage metal-aluminyl complexes and Group 14 dimetallenes and dimetallynes in the framework of alkyne activation recently emerged as well. Indeed, amido-digermylene **3** has been reported to be involved in cycloaddition reactions with terminal alkynes, such as phenylacetylene, leading to the formation of syn alkyne insertion products such as **7**.[16,17] Recently, Aldridge and coworkers showed, again in strict analogy with **3**, that the copper-aluminyl complex **8** (which possesses an electron-sharing poorly polarized Cu–Al bond[2] and reacts with CO_2 similarly to **1**[20,21]) reacts with 3-hexyne in a very similar fashion to **3**, leading to the formation of the *syn* alkyne insertion product **10** under kinetic control.[18]

[a] Dr. D. Sorbelli, Prof. Dr. P. Belanzoni
Department of Chemistry, Biology and Biotechnologies
University of Perugia
Via Elce di Sotto, 8, 06123 Perugia (Italy)
E-mail: diegosorbelli00@gmail.com
paola.belanzoni@unipg.it

[b] Dr. D. Sorbelli, Dr. L. Belpassi, Prof. Dr. P. Belanzoni
CNR Institute of Chemical Science and Technologies "Giulio Natta" (CNR-SCITEC)
Via Elce di Sotto, 8, 06123 Perugia (Italy)
E-mail: leonardo.belpassi@cnr.it

Supporting information for this article is available on the WWW under https://doi.org/10.1002/chem.202203584

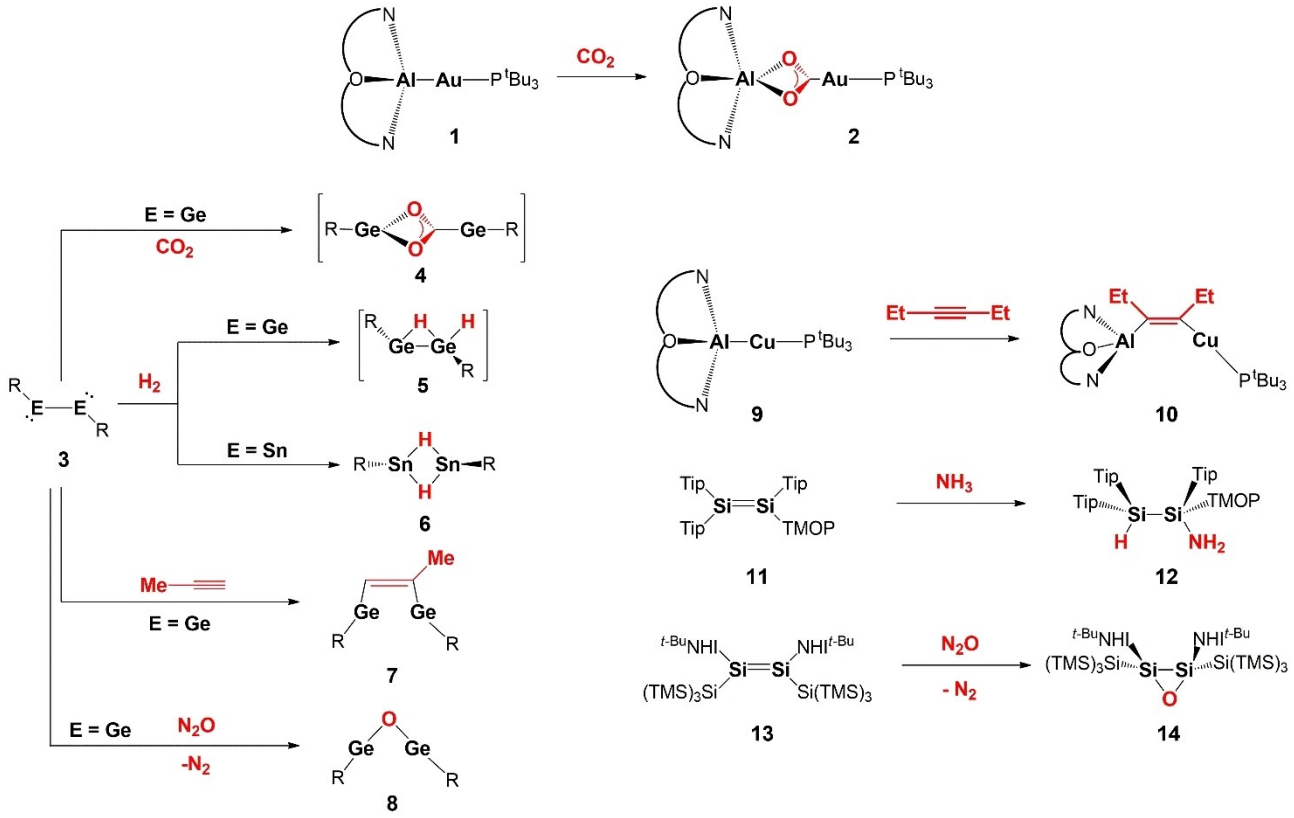

Scheme 1. Experimental reactivity of the [^{t}Bu$_3$PAuAl(NON)] complex with CO_2 (**1**-**2**).[1] Examples of experimental reactivity of Group 14 diamido-metallenes (R = N(Ar$^{\#}$)(SiMe$_3$); Ar$^{\#}$ = 2,6-(CHPh$_2$)$_2$-4-MeC$_6$H$_2$)) with small molecules (CO_2, H_2, phenylacetylene, N_2O) (**3**–**8**).[8–13,15–17] Experimental reactivity of the [^{t}Bu$_3$PCuAl(NON)] complex with 3-hexyne (**9**–**10**).[18] Examples of experimental reactivity of disilenes (Tip = 2,4,6-triisopropylphenyl, TMOP = 2,4,6-trimethoxyphenyl, NHI = N-heterocyclic imine) with NH_3 and N_2O (**11**–**14**).[19]

The eye-catching analogies illustrated here between E–E and Au/Cu–Al bonds, in terms of both bonding features and related reactivity, suggest that gold-aluminyl complexes may be versatile systems for activating either stoichiometrically or catalytically a wide range of small molecules. Note that, on a more general context, the interest around small molecule activation processes mediated by bimetallic systems in a cooperative way is currently of extreme interest due to the high tunability of the metal-metal bonding features.[22,23]

One attractive perspective concerns the activation of E–H (E = O, N) bonds in water and ammonia, respectively. An efficient activation of O–H bonds in water, for instance, is a crucial initial step for the production of dihydrogen from water splitting.[24–26] Similarly, in situ production of dihydrogen via liquid organic hydrogen carriers (LOHCs) requires an efficient O–H bond activation to work in mild conditions.[27,28] In general, it is clear that increasing the efficiency of such processes is key in nowadays critical environmental scenario, allowing to produce fuel, dihydrogen, from extremely abundant and cheap sources, such as water. Similarly, N–H activation processes of the primary amine feedstock, ammonia, are extremely important from an industrial perspective. In principle, NH_3 could be easily used as a versatile starting building block for a plethora of chemicals (pharmachemicals, polymer additives, base chemicals, industrial amines).[29,30] The issue is that the processes that target the N–H activation in NH_3 are in general very limited and become practically unexplored in the framework of transition-metal homogeneous catalysis, due to the high coordinating ability of NH_3.[29,31] Clearly, this state-of-the-art demonstrates the high importance of finding new strategies for its synthetic utilization, especially via selective homogeneous catalysis. Note that, for instance, disilene **11** (Scheme 1) has been reported to efficiently activate N–H bonds in ammonia, leading to the hydroamminated species **12**.[19]

On the other hand, activation and capture of environmentally problematic small molecules is of high interest due to their increasing anthropogenic emissions. Among others, sulfur dioxide (SO_2) is a reactive molecule that is not only a source of environmental pollution, but it also represents an hazard to human health.[32–34] SO_2 comes as a waste from several anthropic activities and the plans for reducing its emissions are not homogeneous worldwide.[34] Furthermore, SO_2 is an S-containing feedstock for chemicals, thus strategies for its activation and capture are of high interest.[34]

The situation is even more critical for nitrous oxide (N_2O). This compound is a greenhouse gas with a global warming potential of more than 300 CO_2 equivalents[35] and it represents the main contribution to ozone depletion.[36,37] Agricultural activities represent the main source of anthropogenic N_2O in the atmosphere[35,38] and, unfortunately, N_2O is kinetically inert,

since its reduction to N_2 features a very high activation barrier (60 kcal/mol ca.)[39–41] Clearly new strategies for its capture, activation and removal are particularly attractive, especially since it can be in principle also used as a synthetic reagent, for instance with the role of O-atom donor.[42,43] Note, again, that the efficient reduction of N_2O with Group 14 dimetallenes has been extensively reported (see as examples **8** and **14** in Scheme 1)[8,9,19] and that, in general, there is considerable interest around the exploration of novel N_2O cooperative bimetallic activation processes, both from a biomimetic and a synthetic perspective.[44]

Considering the unique properties of electron-sharing Au–Al bonds in gold-aluminyl complexes and their reactivity with small molecules of various nature, the aim of this work is to explore their reactivity with other small molecules, namely NH_3, H_2O, SO_2 and N_2O, exploiting the electronic structure of the involved species and their features, while also trying to explore possible catalytic routes in this context. The results are encouraging, showing that the activation of these substrates is in principle both thermodynamically and kinetically feasible in all cases. Furthermore, a computational screening reveals that gold-aluminyl complexes may be ideal catalysts for oxygen-atom transfer catalysis involving reduction of N_2O and oxidation of substrates such as phosphines and boranes. Experiments validating these results are clearly desirable.

Results and Discussion

O–H and N–H bond activation in H_2O and NH_3

In Figure 1 the pathways for the reaction of the [^{t}Bu$_3$PAuAl(NON)] complex with NH_3 (blue and dark cyan paths) and H_2O (orange and red paths) are reported. The involved stationary point structures are depicted in Figure 2.

Inspection of the reaction profiles clearly reveals that the two reactions present qualitatively similar features.

Both reactions consist of a one-step activation of the N–H and O–H bonds of ammonia and water, respectively, leading to the formation of the corresponding H singly-bridged products PC_{NH3} and PC_{H2O}. In these products, complete E–H (E = O, N) bond dissociation has occurred, with the NH_2/OH moieties bound to the aluminium site. Furthermore, in both cases, the product can be formed via two different pathways, i.e. with NH_3/H_2O interacting closer either with the gold (TS_{NH3} and TS_{H2O}, blue and orange pathway, respectively) or aluminium (TS_{NH3}' and TS_{H2O}', dark cyan and red pathway, respectively) sites.

Quantitatively, the results reported in Figure 1 suggest that, independently of the pathway, the activation of E–H bonds is both kinetically and thermodynamically feasible. The formation of PC_{NH3} and PC_{H2O} is exergonic (−9.3 and −20.8 kcal/mol, respectively) and the activation barrier is found to be lower than 15 kcal/mol for all pathways, suggesting an accessible process even in mild experimental conditions.

Differences between the O–H and N–H bond activation pathways arise on a quantitative ground. According to the results reported in Figure 1, the O–H bond activation reaction for water is found to be more favorable for both pathways: the

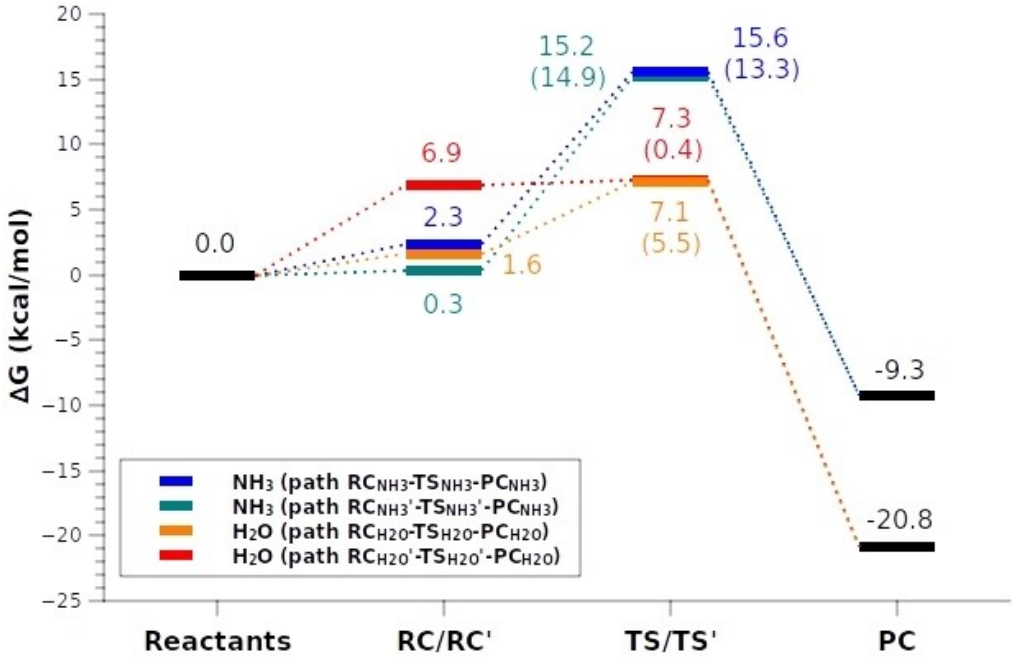

Figure 1. Free energy reaction profiles for the N–H (blue and dark cyan profiles) and O–H (orange and red profiles) bond activations in ammonia and water, respectively, by the [^{t}Bu$_3$PAuAl(NON)] complex. ΔG values refer to the energy of the separated reactants taken as zero. Activation free energy barriers are reported in parentheses.

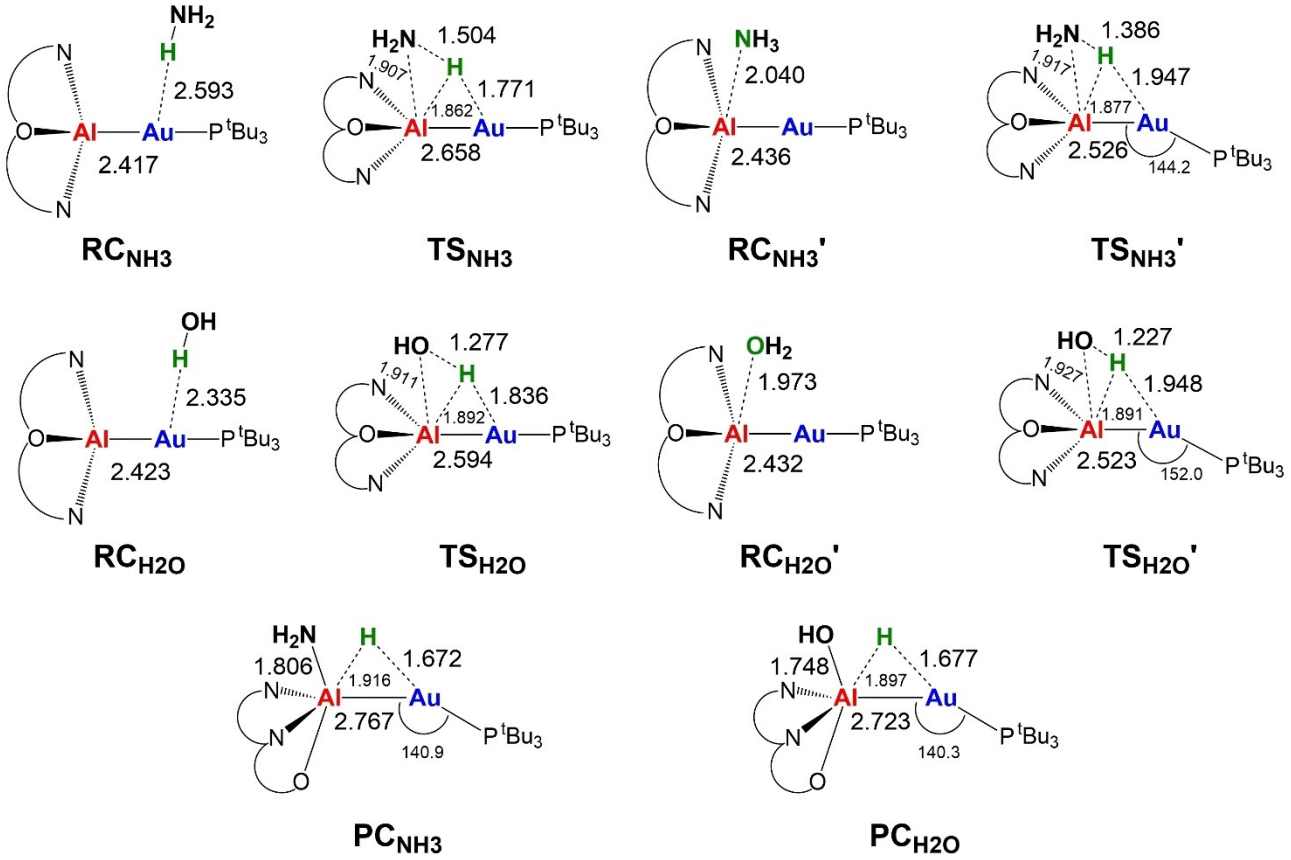

Figure 2. Sketched stationary point structures along the paths of Figure 1 with selected interatomic distances (Å) and bond angles (degrees).

activation barriers (5.5 and 0.4 kcal/mol via TS_{H2O} and TS_{H2O}', respectively) are significantly lower than those for the N–H activation (13.3 and 14.9 kcal/mol via TS_{NH3} and TS_{NH3}', respectively). Analogously, PC_{H2O} is found to be significantly more stable than the corresponding PC_{NH3} (−20.8 vs. −9.3 kcal/mol, respectively).

Analogies and differences in the reaction pathways can be rationalized by carrying out the Activation Strain Model[45–47] (ASM) analysis. To this aim, we performed a relaxed scan of the Potential Energy Surface (PES) in the vicinity of each TS and then carried out the ASM analysis on each relaxed PES point (see the Computational Details section for insights on the PES scan). The resulting Activation Strain Diagrams (ASDs) are reported in Figure 3, while the related numerical data are collected in Table S1 in the Supporting Information.

The ASM results agree with the free energy pathways reported in Figure 1, depicting an overall more favorable activation via TS_{H2O}/TS_{H2O}' with respect to TS_{NH3}/TS_{NH3}'. The ASM decomposition reveals that the balance between distortion penalty and interaction stabilization is clearly favoring the O–H bond activation in water via TS_{H2O}/TS_{H2O}'. In detail, as shown in Figure 3 (and in Table S1 in the Supporting Information), the distortion penalty (top right in Figure 3), while being slightly lower for TS_{NH3}, is generally comparable in all the reaction pathways. As a result, (see Figure 3, bottom), the stabilizing interaction energy is discriminating the overall relative energy of the pathways. In fact, it can be clearly seen that, for most parts of the sampled PES, the interaction energy is significantly lower (more negative) for TS_{H2O}/TS_{H2O}', thus being able to more efficiently counterbalance the unfavorable strain penalties and, eventually, to lead to a lower activation barrier (and related energy path) for both TS_{H2O} and TS_{H2O}'.

Clearly, the complex-water interactions are crucial in providing a more efficient formation of PC_{H2O} via TS_{H2O}/TS_{H2O}'. For this reason, it is worth analyzing in detail the nature of the interactions occurring between the substrate and the gold-aluminyl complex at each transition state through the Energy Decomposition Analysis (EDA, results are collected in Table S2 in the Supporting Information),[48–50] Charge Displacement (CD)[51–53] and Natural Orbitals for Chemical Valence[54] (NOCV) tools. Complete NOCV results are reported in Figures S1–S8 in the Supporting Information. Main results are compared in Figure 4.

From inspection of Figure 4 (and Figures S1–S8 in the Supporting Information) it can be easily inferred that the H_2O- and NH_3-complex interactions are qualitatively analogous for all transition states. In both cases, two main NOCV deformation densities ($\Delta\rho_1'$ and $\Delta\rho_2'$) are found to be the driving forces of the interaction at the transition states under study. The analysis reveals that these components are very much analogous to those discussed in previous works concerning the CO_2-[^{t}Bu$_3$PAuAl(NON)][2] and H_2-[^{t}Bu$_3$PAuAl(NON)][14] interactions. In

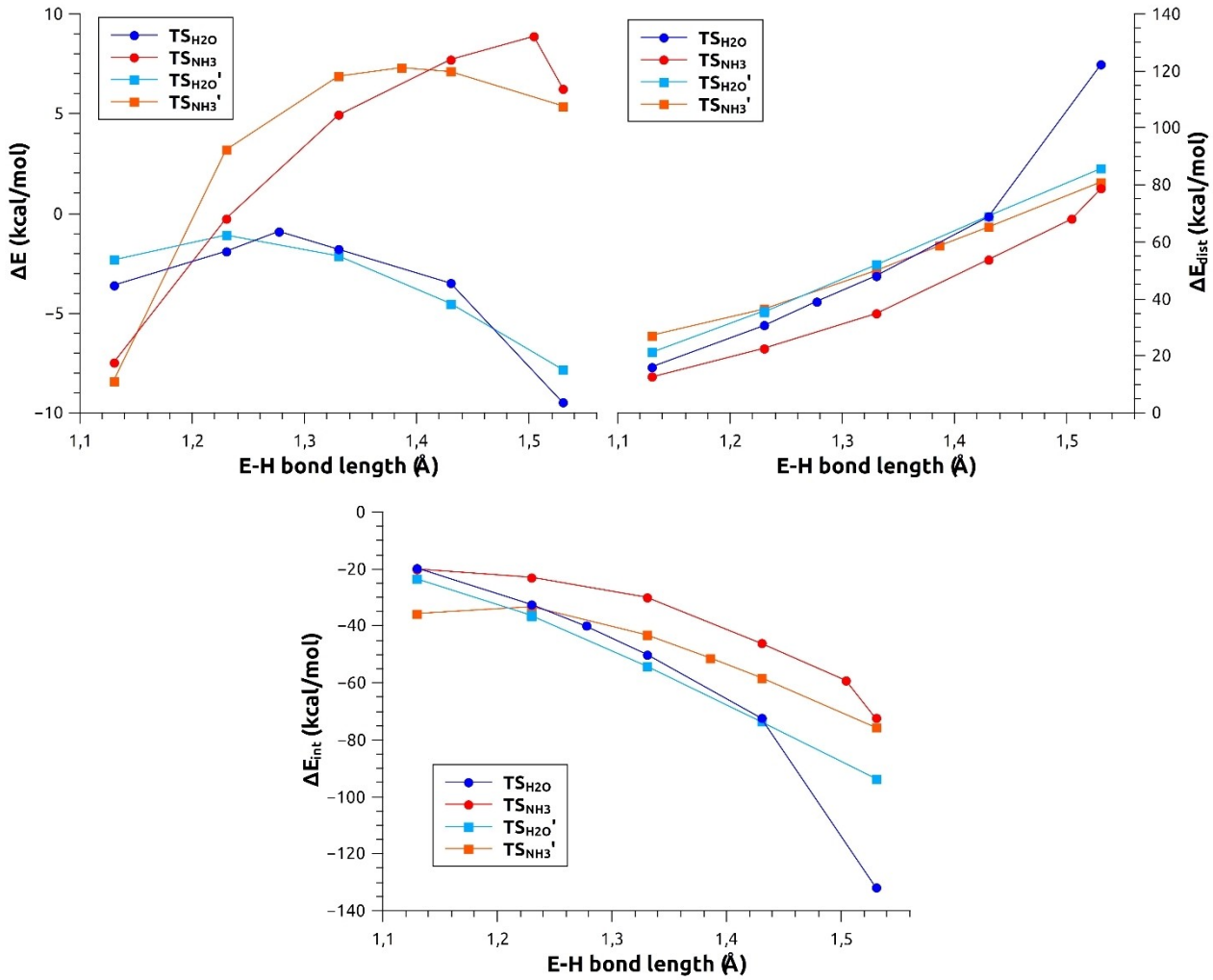

Figure 3. Activation Strain Diagrams (ASD) for the Potential Energy Surface (PES) region neighboring TS_{H2O}, TS_{H2O}', TS_{NH3}, TS_{NH3}'. Overall relative energies (ΔE, top left), overall distortion penalties (ΔE_{dist}, top right) and interaction energies (ΔE_{int}, bottom) are reported for each point of the relaxed PES. See the Computational Details section for details on the PES relaxed scan and the Methodology section in the Supporting Information for a brief overview of the Activation Strain Model.

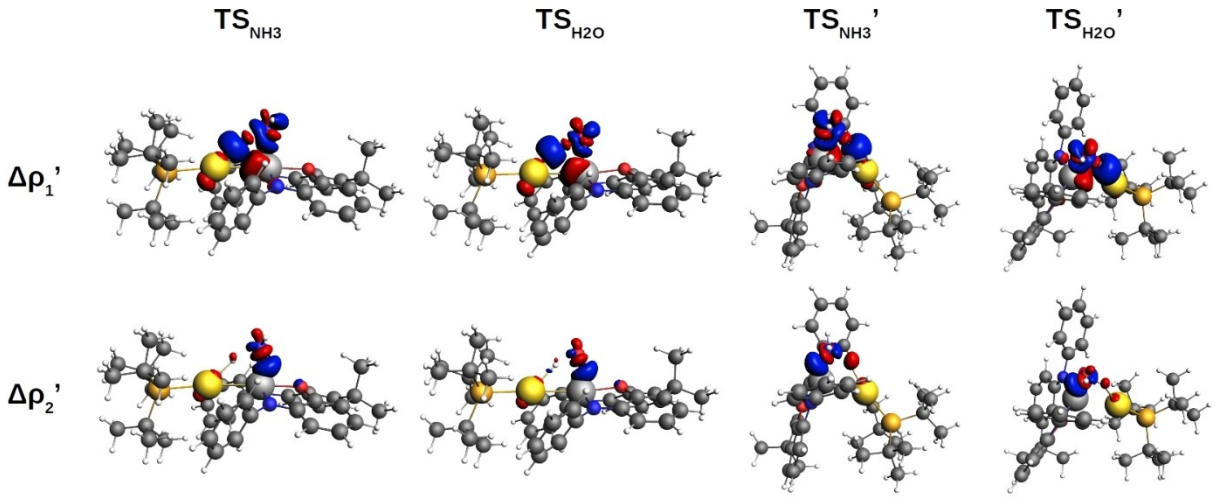

Figure 4. Main results of the NOCV analysis of the $[NH_3]$–$[^tBu_3PAuAl(NON)]$ and $[H_2O]$–$[^tBu_3PAuAl(NON)]$ interaction at TS_{NH3}/TS'_{NH3} and TS_{H2O}/TS'_{H2O}, respectively. Charge flux is red→blue. Isovalue is 3 me/a_0^3 for all isosurfaces.

detail, $\Delta\rho_1'$ consists of an accumulation of electron density at the LUMO of water and ammonia, mainly localized on the O–H and N–H bonds, respectively. Depletion regions are clearly visible on both gold and aluminium sites, indicating actual depletion of electron density from the highest σ occupied molecular orbitals of the complex, mainly localized at the Au–Al bond site (see Figures S1, S3, S5 and S7 in the Supporting Information). The second deformation density, $\Delta\rho_2'$, is induced by the Lewis behavior of Al, as can be envisaged by the accumulation pattern at the Al site. In particular, accumulation of electron density occurs at the LUMO of the complex, which displays large contributions from Al $3p_z$ empty orbital, which is found to be populated by the lone pair on the N/O atom (see Figures S2, S4, S6 and S8 in the Supporting Information).

Ultimately, it is interesting to explore if the gold-aluminyl complex is prone to induce a homolytic or heterolytic bond breaking, resulting in a radical pair stabilization mechanism, in analogy with the reactivity with H_2 we reported very recently.[14] To verify this hypothesis, we evaluate the relative stability of [^{t}Bu$_3$PAu(μ-H)Al(NON)] and [^{t}Bu$_3$PAuAl(EH$_x$)(NON)] species (EH$_x$ = OH, NH$_2$) in their open-shell radical and closed-shell charged forms. This simple model allows us to assess the extent of stabilization provided by the gold-aluminyl complex to H·/H$^+$, OH·/OH$^-$, NH$_2$·/NH$_2^-$ species, to evaluate the most suitable E–H bond fragmentation scheme (i.e. homolytic or heterolytic).

The results, reported in Figures S9 and S10 in the Supporting Information, suggest that the reactivity of the [^{t}Bu$_3$PAuAl(NON)] complex with H_2O and NH_3 is indeed best described as a radical pair recombination mechanism resulting from a homolytic E–H bond dissociation. In fact, from Figures S9 and S10 it can be inferred that the formation of the open-shell [^{t}Bu$_3$PAu(μ-*H*)Al(NON)]· species from OH· dissociation has an associated energy of 241.0 kcal/mol, while the formation of closed-shell [^{t}Bu$_3$PAu(μ-*H*)Al(NON)]$^+$ species from OH$^-$ dissociation is less favorable, with an associated energy of 324.4 kcal/mol. Similarly, formation of the [^{t}Bu$_3$PAuAl(OH)(NON)]· species is favored over [^{t}Bu$_3$PAuAl(OH)(NON)]$^-$ (the associated formation energies are 84.2 and 272.9 kcal/mol, respectively). Analogously, the formation of the [^{t}Bu$_3$PAu(μ-*H*)Al(NON)]· species from NH$_2$· dissociation has an associated energy of 107.2 kcal/mol, while the dissociation of NH$_2^-$ produces a less stable [^{t}Bu$_3$PAu(μ-*H*)Al(NON)]$^+$ species (formation energy is 141.6 kcal/mol). Similarly, the dissociation of H· leading to the [^{t}Bu$_3$PAuAl(NH$_2$)(NON)]· radical is more favored energetically (83.7 kcal/mol) with respect to the formation of the anionic [^{t}Bu$_3$PAuAl(NH$_2$)(NON)]$^-$ species from H$^+$ dissociation (275.4 kcal/mol).

The enhanced ability of the gold-aluminyl complex to cooperatively stabilize H·, OH· and NH$_2$· species is consistent with the spin density associated with the [^{t}Bu$_3$PAuAl(OH)(NON)]· and [^{t}Bu$_3$PAuAl(NH$_2$)(NON)]· species (Figure S10), where the unpaired electron is found to be almost entirely localized on gold and aluminium atoms with no unpaired electron density on the bound OH and NH$_2$ moieties.

These results predict the gold-aluminyl complex to efficiently activate and induce homolytic N–H and O–H bond breaking in both H_2O and NH_3. This finding, coupled with the previously reported radical-like reactivity of the complex,[2–5,14] as well as with the actual diradical reactivity of analogous iron-aluminyl species with CO_2,[55] leads to a reactivity model in which the electron-sharing Au–Al bond is the driving force of an efficient radical-like mechanism towards E–H bond activation in water and ammonia.

SO_2 capture and N_2O reduction

In Figure 5 the profiles for the reaction of [^{t}Bu$_3$PAuAl(NON)] with SO_2 and N_2O are reported. Structures of all the stationary points are sketched in Figure 6.

As shown by the red profile in Figure 5 (and corresponding structures of the stationary points in Figure 6), the reaction of SO_2 with the [^{t}Bu$_3$PAuAl(NON)] complex is strongly reminiscent of the reactivity of the same complex with CO_2. Indeed, the reaction profile consists of the SO_2 approach at both the Al and Au sites of the complex, resulting in the formation of a cyclic stable intermediate (INT_{SO2}). Subsequently, the second ring-opening step, with the formation of two O–Al bonds and breaking of the Au–Al bond, leads to the insertion product PC_{SO2}. The overall process is highly exergonic (−31.4 kcal/mol) with very low activation barriers for the two steps (3.1 and 5.2 kcal/mol at TSI_{SO2} and $TSII_{SO2}$, respectively), suggesting that the reaction may be easily feasible in mild experimental conditions both kinetically and thermodynamically.

The mechanism for the reaction of [^{t}Bu$_3$PAuAl(NON)] with N_2O is qualitatively different, as displayed in Figure 5 (blue profile). In this case, the reaction occurs through a one-step mechanism, in which N_2O approaches the complex via a unique transition state (TS_{N2O}), where the N_2O oxygen atom interacts with the Al site of the complex and, simultaneously, the central nitrogen atom interacts with the Au site. As a result, N_2 extrusion occurs, resulting in the formation of [^{t}Bu$_3$PAuOAl(NON)] oxo-complex. Thermodynamically, as expected, the reaction is highly exergonic, but, interestingly, the reaction appears to be also accessible from a kinetic standpoint in mild conditions, with a free energy activation barrier of 15.2 kcal/mol (significantly lower than the barrier for the unsupported N_2O reduction[39–41]). Validation of these results by experiment would be thrilling for *i)* the interest in this process for the use of pollutant N_2O as an oxygen-atom donor *ii)* the possible isolation of the [^{t}Bu$_3$PAuOAl(NON)] intermediate, which could not be previously isolated from reaction with CO_2 via CO extrusion.[1,20,21]

Despite the two mechanisms in Figure 5 present highly different features, the substrate-complex interactions appear to be extremely similar to the ones discussed earlier in this work for water and ammonia, as well as previously for CO_2 and H_2, as emerging from the results of the NOCV and CD analyses performed at TSI_{SO2} and TS_{N2O} and illustrated in Figure 7. Complete NOCV results are also shown in Figures S11–S14 in the Supporting Information.

The main results of the NOCV and CD analyses at TSI_{SO2} and TS_{N2O} reported in Figure 7 (and Figures S11–S14 in the Supporting Information) clearly display these analogies. In fact, as can

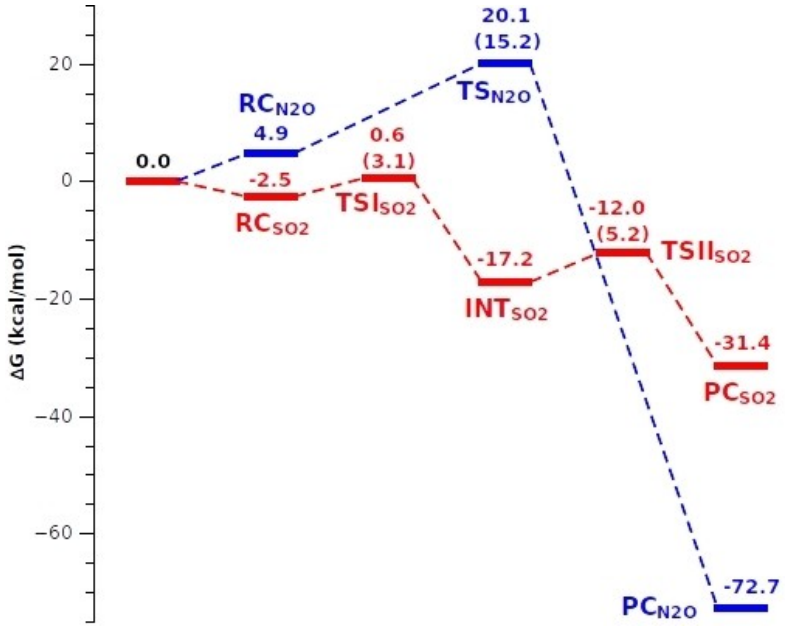

Figure 5. Free energy reaction profiles for the SO_2 capture (red profile) and N_2O reduction (blue profile) by the [^{t}Bu$_3$PAuAl(NON)] complex. ΔG values refer to the energy of the separated reactants taken as zero. Activation free energy barriers are reported in parentheses.

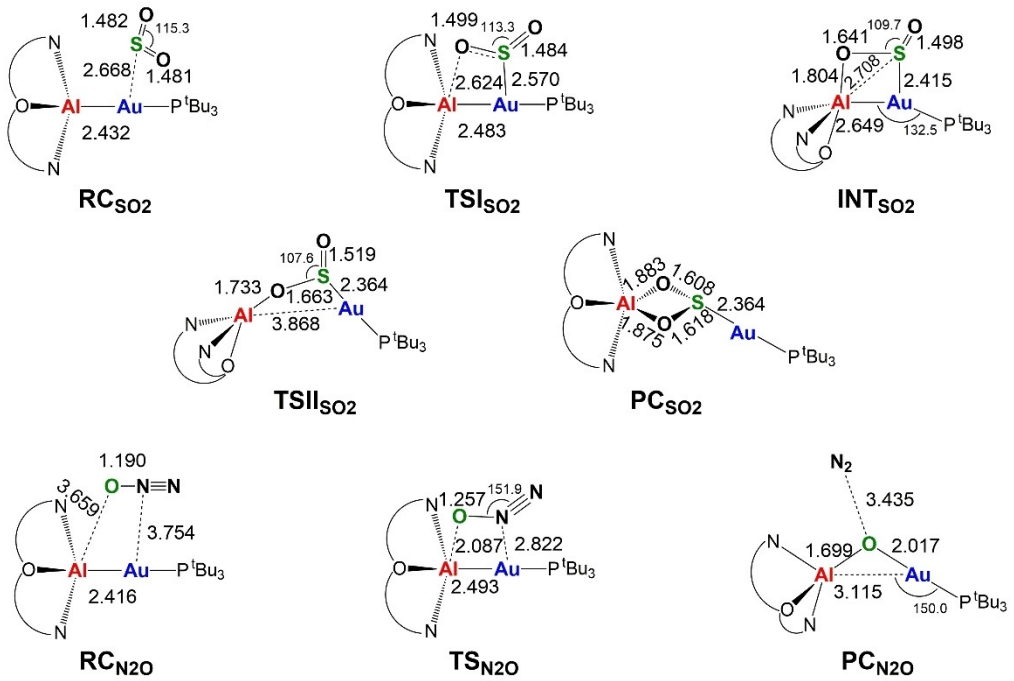

Figure 6. Sketched stationary point structures along the paths of Figure 5 with selected interatomic distances (Å) and bond angles (degrees).

be envisaged from Figure 7 *a)*, the main driving force ($\Delta\rho_1$') of the [SO_2]–[^{t}Bu$_3$PAuAl(NON)] interaction is represented by the charge transfer from the electron-sharing Au–Al bond towards the empty π* molecular orbital of SO_2 (see Figure S11), strongly resembling the interaction scheme depicted for CO_2 in refs [2–5]. Analogously, a second component of the interaction ($\Delta\rho_2$') consists of a charge donation from the filled antibonding π orbital of SO_2 towards the vacant $3p_z$ orbital of Al (Figure 7 *b)* and Figure S12).

The analyses at TS_{N2O}, despite the different reaction mechanism for N_2O reduction, reveal the same forces at play. As shown in Figure 7 *c)*, the main driving force ($\Delta\rho_1$') of the interaction between nitrous oxide and the complex is still found to be the charge transfer from the Au–Al bond towards the

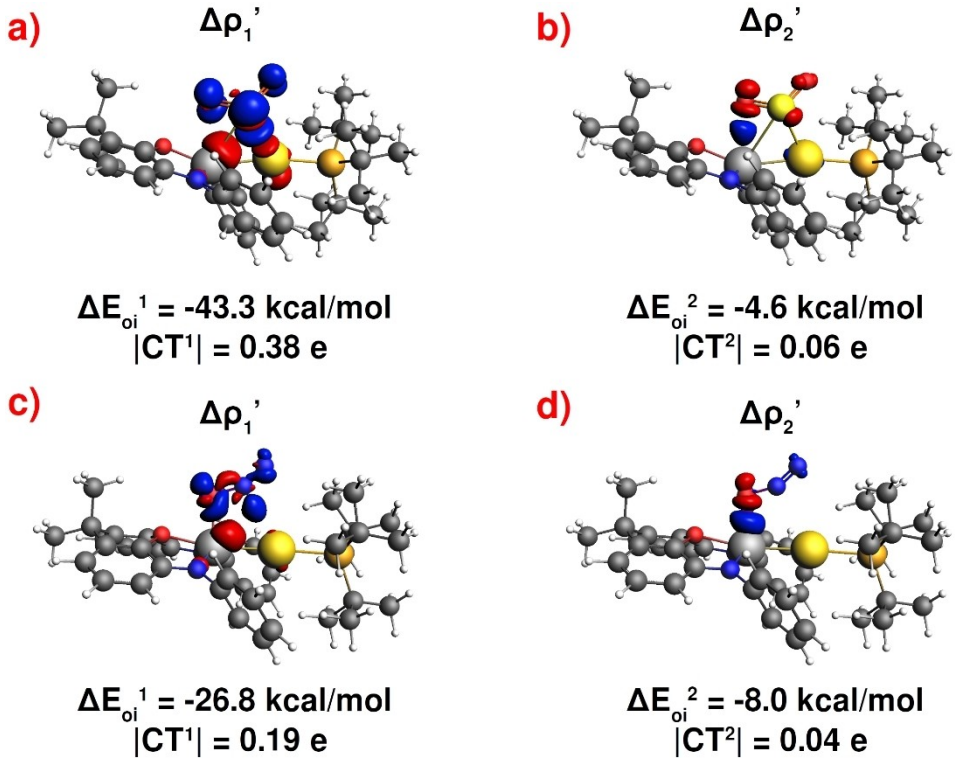

Figure 7. Results of the NOCV analysis of the $[SO_2]$–[^{t}Bu$_3$PAuAl(NON)] (*a–b*) and $[N_2O]$–[^{t}Bu$_3$PAuAl(NON)] (*c–d*) interaction at TSI_{SO2} and TS_{N2O}, respectively. Charge flux is red→blue. Isovalue is 3 me/a_0^3 for all isosurfaces.

empty π* molecular orbital of N_2O (Figure S13). Analogously, the second component ($\Delta\rho_2'$) consists of the charge donation from a filled π orbital of N_2O towards an empty orbital of Al (Figure 7 *d)* and Figure S14).

Interestingly, further inspection of the binding mode of nitrous oxide at TS_{N2O} unveils other peculiarities about the chemistry presented in this work. In fact, as discussed earlier and shown schematically in Figure 6, at TS_{N2O} nitrous oxide displays a μ-1,2-O,N binding to the Au and Al sites, clearly arising, as discussed from Figure 7, from the nature of the complex-N_2O interaction. This coordination mode, however, is uncommon for the reactivity of N_2O with bimetallic (and multimetallic) systems of biological, biomimetic and synthetic nature.[44,56] Indeed, in biological systems, such as in the nitrous oxide reductase enzyme, a μ-1,3-O,N binding is often observed,[56–58] while synthetic and biomimetic bimetallic systems often feature different binding schemes (in several cases they show either a μ-1,1-O binding to the M–M′ unit or initial O-coordination to one metal site and subsequent N_2 extrusion).[59,60]

In light of the recently discussed peculiar topological features of the potential energy surface (PES) of the [^{t}Bu$_3$PAuAl(NON)] complex with CO_2, revealing the presence of geometrically different but almost isoenergetic transition states along the same reaction coordinate,[3] and prompted by the differences above described, we explored the features of the PES neighboring TS_{N2O}. A graphical representation of the PES is depicted in Figure 8, while the numerical data for the PES exploration are reported in Table S3 in the Supporting Information.

As can be inferred from Figure 8 (and from the related numerical data reported in Table S3 in the Supporting Information), the topology of the PES around TS_{N2O} is particularly flat, despite inducing significant changes in the N_2O coordination. Surprisingly, in analogy with the reactivity with carbon dioxide,[3] the flat topology of the PES allows to locate another transition state (labeled as TS_{N2O}*) in which N_2O displays a different binding mode to the complex, as shown from the insets of Figure 8. Indeed, TS_{N2O}* shows a coordination mode closer to the μ-1,1-O binding often observed for synthetic bimetallic systems, with a large Au–N distance (3.953 Å) and a shorter Al–O bond (1.975 Å). Interestingly, TS_{N2O} and TS_{N2O}* exhibit a similar imaginary frequency (−299.1 and −352.0 cm^{-1}, respectively), an analogous nature of the associated vibrational mode, involving concerted O–Al and O–N stretching modes and, notably, almost the same energy. In fact, TS_{N2O} and TS_{N2O}* are practically isoelectronic, differing by 1.9 kcal/mol in terms of electronic energy and by 0.8 kcal/mol in terms of Gibbs' free energy. All these evidences, coupled with the fact that, as can be clearly seen from Figure 8 and Table S3, the two local maxima corresponding to TS_{N2O} and TS_{N2O}* are connected by a practically flat portion of the PES, clearly suggest that this is a case in which two almost isoenergetic transition states are located along the same reaction coordinate. The analogies between TS_{N2O} and TS_{N2O}* can be further inferred from the NOCV analysis of the complex-N_2O interaction at TS_{N2O}* (see

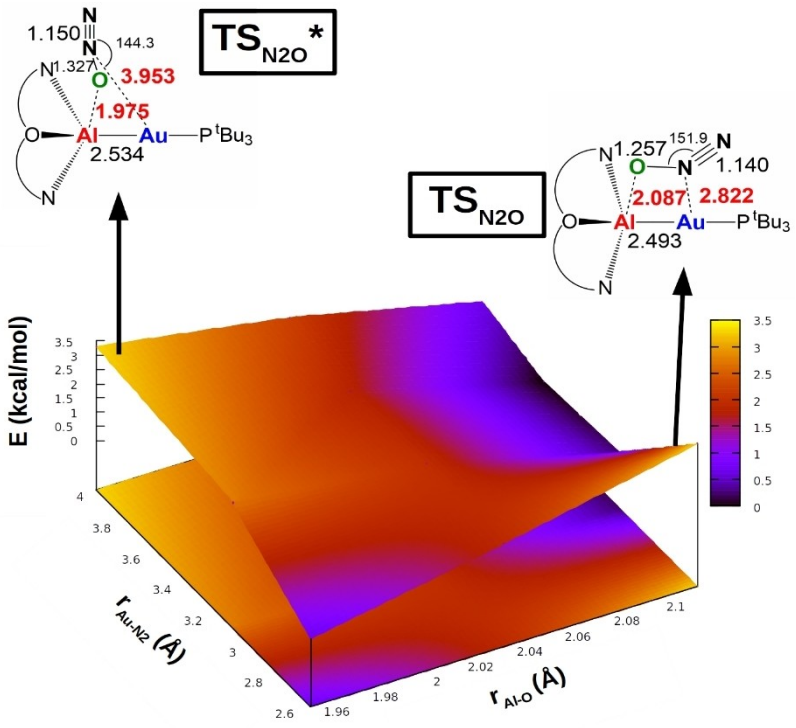

Figure 8. Potential energy surface (PES) in the region neighboring TS_{N2O}. *Insets:* Position on the PES and schematic structure of TS_{N2O} and TS_{N2O}*. Energy has been shifted in each case according to the minimum energy structure.

Figure S15 in the Supporting Information), which clearly shows that the main component driving the interaction is the electron charge transfer from the Au–Al bond towards the LUMO of N_2O, supplemented with the charge transfer from the HOMO-1 of the substrate towards the $3p_z$ vacant orbital of the complex.

These findings seem to actually indicate that the sole inspection of the N_2O binding modes to bimetallic systems, which has often been used as an indirect indicator of the nature of the N_2O-metal interaction,[56] may not be a good probe for N_2O activation when, as happens in this case, the cooperative bimetallic character of the reactivity induces the presence of a peculiar flat topology of the related PES.

Furthermore, in this case as well it is worth investigating if both SO_2 capture and N_2O reduction occur via a radical-like mechanism. Application of an adapted scheme (see Scheme S1 in the Supporting Information) for the formation of PC_{SO2} and PC_{N2O} from radical or closed-shell charged gold and aluminyl fragments reveals that a radical-like mechanism is likely for the reaction with both SO_2 and N_2O reduction. As displayed in Table S4 in the Supporting Information, overall formation of PC_{SO2} is more favorable starting from open-shell radical [^{t}Bu$_3$PAu]· and [Al(NON)]· fragments (ΔE is −128.6 kcal/mol) with respect to closed-shell fragments, where the less negative formation energy indicates less stable starting fragments (ΔE is −157.4 kcal/mol). Similarly, PC_{N2O} is formed more favorably starting from radical gold and aluminyl fragments (ΔE is −159.2 kcal/mol) with respect to the closed-shell charged ones (ΔE is −197.1 kcal/mol).

Clearly, these results further corroborate the general applicability of the reactivity scheme depicted in the previous section and works,[2–5,7,14] which might be safely extended to explain the reactivity of gold-aluminyl complexes towards other small molecules of various nature.

Catalytic reduction of N_2O: examples of oxygen-atom transfer catalysis

As mentioned in the introduction, nitrous oxide, other than being a pollutant and a highly concentrated greenhouse gas, can be used as oxidant in the framework of oxygen-atom transfer catalysis.[43]

In this context, having established that the conversion of gold-aluminyl complex **1** to the [^{t}Bu$_3$PAuOAl(NON)] oxo-complex via N_2O reduction is predicted to be both thermodynamically and kinetically accessible, it is worth exploring if such stoichiometric process can be converted into a catalytic one. In particular, [^{t}Bu$_3$PAuOAl(NON)] can be seen as a source of oxygen atoms, thus potentially enabling the role of **1** as catalyst for several crucial processes.

Motivated by this perspective, the concluding part of this work is dedicated to the computational thermodynamic screening of the re-conversion of [^{t}Bu$_3$PAuOAl(NON)] into initial complex **1** via oxygen-atom transfer towards suitable substrates. The considered reactions for this thermodynamic screening are reported in Scheme 2.

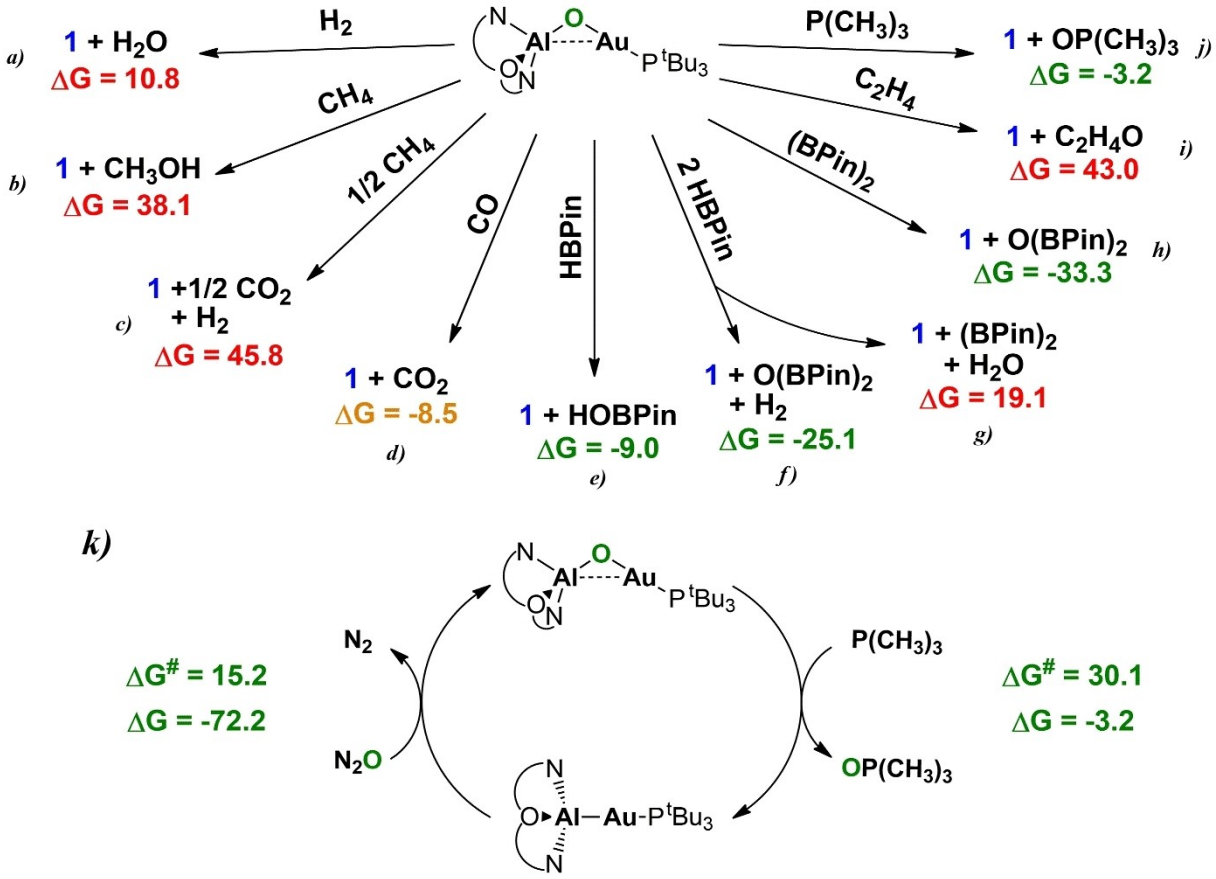

Scheme 2. Schematic representation of the reactions for the re-conversion of the [^{t}Bu$_3$PAuOAl(NON)] oxo-complex to **1** using different reductants as substrates together with the corresponding relative Gibbs' free energy values (ΔG) in kcal/mol (*top*, *a–j*). Calculated cycle for the catalytic joint reduction of N_2O and oxidation of trimethylphosphine $P(CH_3)_3$ catalyzed by **1** together with the Gibbs' free energy activation barriers ($\Delta G^{\#}$) and relative stabilities (ΔG) in kcal/mol (*bottom*, *k*).

As can be readily seen from Scheme 2, some reactions are not accessible thermodynamically. For instance, oxidation of dihydrogen to water (*a*) is found to be endergonic (+10.8 kcal/mol) and, similarly, oxidation of methane to either methanol or CO_2+H_2 (*b* and *c*, respectively) is highly endergonic as well (38.1 and 45.8 kcal/mol, respectively). Oxidation of CO to CO_2 (*d*), conversely, is predicted to be exergonic (−8.5 kcal/mol). Nonetheless, we can already assume that in this case **1** will not efficiently work as a catalyst since its catalytic activity would be easily inhibited by its affinity with the final product of the reaction (CO_2).

The oxidation of pinacolborane (HBPin) (pin = pinacolate: 2,3-dimethyl-2,3 butanediolate) appears to be a thermodynamic accessible route instead. Recently, several examples of analogous reactivity using boranes as sacrificial reductants have been reported.[61–63] One equivalent of HBPin is predicted to be converted exergonically to the corresponding hydroxide HOBPin (*e*, −9.0 kcal/mol), while two equivalents of HBPin are converted to the bis-boryloxide $O(BPin)_2$ and dihydrogen (*f*) with an even more exergonic reaction (−25.1 kcal/mol). Notably, formation of bis(pinacolato)diboron $BPin_2$ and water (*g*) is highly endergonic (19.1 kcal/mol), suggesting that reactions with formation of water as a product are not favorable in this context. Ultimately, the reaction of **1** with $BPin_2$ yielding the bis-boryloxide $O(BPin)_2$ as the only product (*h*) is found to be even more exergonic (−33.3 kcal/mol).

Clearly, the perspective of catalytically reduce N_2O and simultaneously produce species such as $O(BPin)_2$, which is a valuable precursor for several synthetic pathways[64,65] is thrilling. For this reason, it would be interesting to explore the actual catalytic mechanism (including kinetics) in order to get preliminary insights on its possible catalytic activity. Nonetheless, the stoichiometry of the reaction and its selectivity are not very straightforward and the reaction mechanism can become quite complicated without experimental insights on the reactivity, as recently discussed in some works.[62,63]

Still as promising and more computationally approachable, other interesting processes in this context are the catalytic epoxidation of alkenes and oxidation of phosphines. However, while the reaction step involving the catalytic epoxidation of ethylene (*i*) is predicted to be highly endergonic (+43.0 kcal/mol), thus strongly suggesting a poor catalytic activity of **1** in this framework, the conversion of trimethylphosphine $P(CH_3)_3$ to the $OP(CH_3)_3$ oxide (*j*) is predicted to be exergonic (−3.2 kcal/mol). In the latter case, we were also able to explore computationally a possible reaction mechanism (*k*), which results in a

one-step oxidation via a concerted transition state with a calculated activation barrier at 298 K of 30.1 kcal/mol. Considering the generally high experimental temperatures in which both catalytic N_2O reduction and phosphine oxidation occur,[42,43] an activation barrier of 30.1 kcal/mol at 298 K appears to be promising for a feasible process upon rational control of the experimental conditions.

The results reported here pave the way for the experimental exploration of the reactivity of gold complexes with the new-generation aluminyl ligands not only for the stoichiometric activation of a plethora of small molecules, but also, as in the case of nitrous oxide, for their use as catalysts within an unprecedented mode for gold catalysis.

Conclusions

In this work, based on the exceptional features of gold-aluminyl complexes and inspired by their similarities with Group 14 dimetallenes, which have been reported to activate efficiently a plethora of small molecules, we computationally assess the reactivity of gold-aluminyl complexes in the framework of small molecule activation processes. In particular, we study the stoichiometric activation of N–H and O–H bonds in ammonia and water, respectively, by the [^{t}Bu$_3$PAuAl(NON)] complex, as well as the activation of SO_2 and N_2O, also motivated by the either industrial and/or environmental interest around the activation of these substrates.

The results of the computational mechanistic analysis reveal that all processes are thermodynamically and kinetically accessible, with exergonic formation of the activation products and free energy barriers lying way below 20 kcal/mol. These factors indicate that, in principle, such processes are experimentally feasible in relatively mild experimental conditions. A joint electronic structure analysis reveals a well-defined trend in the reactivity of gold-aluminyl complexes. In fact, both E–H (E = O, N) bond activations and reactivity with SO_2 and N_2O, which, on the paper, are substrates with very different electronic properties, occur with the nucleophilic role of the electron-sharing Au–Al bond as a driving force, supported by the electrophilic behavior of the Al site. This evident analogy with CO_2 (and H_2) now allows to establish this reactivity pattern as a general mark of the reactivity of this class of complexes, highlighting their versatility. Furthermore, in all cases we quantitatively assessed that all these processes occur via a radical-like mechanism, which appears as a general feature of gold-aluminyl complexes as well.

Interestingly, further exploration of the Potential Energy Surface (PES) around the transition state for the reactivity with N_2O clearly revealed that the PES displays a very flat topology in this region. Notably, this feature eventually leads to detect two transition states, which, despite showing remarkable geometrical differences, are located along the same reaction coordinate and have practically the same energy. This finding, in the context of the variety of N_2O binding modes reported in the literature for bimetallic systems, highlights that the coordination modes of nitrous oxide to metal sites in a cooperative bimetallic activation may not be solid indicators of the nature and extent of the metal-N_2O interaction.

In the end, upon thermodynamic analysis, the study also reveals that the reduction of nitrous oxide can occur together with an oxygen-atom transfer towards suitable substrates in a catalytic fashion. In particular, N_2O can behave as oxidant towards substrates like phosphines (and boranes) by relying on the catalytic activity of the gold-aluminyl complex, which makes the process in principle accessible.

Clearly, this contribution strongly calls for experimental confirmation of the computationally investigated reactivities, which would represent a series of unprecedented chemical processes in the framework of gold molecular chemistry and catalysis.

Computational Details

Complex **1** has been slightly simplified at the NON site by replacing the two tert-butyl groups at the peripheral positions of the dimethylxanthene moiety with hydrogen atoms and the two Dipp substituents on the nitrogen atoms with phenyl groups. The effect of the modelling for this class of complexes has been extensively evaluated in refs. [1,2] where the same computational set up as that used in the present work was applied. Good agreement with experimental data was found for geometries and in general both the reaction mechanism and the electronic structure calculations show negligible deviations due to the structural simplifications used. All geometry optimizations and frequency calculations on optimized structures (minima with zero imaginary frequencies and transition states with one imaginary frequency) have been carried out using the Amsterdam Density Functional (ADF) code[66,67] in combination with the related Quantum-regions Interconnected by Local Description (QUILD) program.[68] The PBE[69] GGA exchange-correlation (XC) functional, the TZ2P basis set with a small frozen core approximation for all atoms, the ZORA Hamiltonian[70–72] for treating scalar relativistic effects, and the Grimme's D3-BJ dispersion correction were used.[73,74] Solvent effects were modeled by employing the Conductor-like Screening Model (COSMO) with the default parameters for toluene as implemented in the ADF code.[75] The same computational setup has also been used for the EDA, CD-NOCV, and ASM calculations. This computational protocol has been used in refs. [1,2] to study the [^{t}Bu$_3$PAuAl(NON)] and [^{t}Bu$_3$PAuCO$_2$Al-(NON)] complexes and to investigate the mechanisms of the CO_2 insertion reaction in similar compounds featuring gold and Group 13 elements.[3–5]

Note that generally, as advised for the application of the Activation Strain Model,[47] the use of Intrinsic Reaction Coordinate (IRC) calculations to monitor the evolution of distortion and interaction contributions along the reaction coordinate is recommended. Unfortunately, as we have previously demonstrated, the IRC approach is unable to yield the correct connectivity between transition states and minima in this context due to the flat and complex topology of the Potential Energy Surface (PES).[3,4,76] This issue of the IRC approach has also been previously discussed within a more general perspective in the literature, see for instance ref. [77].

For this reason, we resort instead in exploring the PES along the E–H reaction coordinate around each transition state. In particular, we sample a substantial portion of the PES in the vicinity of each TS by scanning the E–H bond length in the 1.13–1.53 Å range and, then, we perform the ASM analysis on the resulting relaxed points of the PES. This approach allows us to still correctly study the

evolution of interaction and distortion contributions along the reaction path by avoiding any issue with the use of the IRC approach.

Acknowledgements

The authors would like to acknowledge the funding support from the Ministero dell'Università e della Ricerca (MUR, project AMIS, through the program "Dipartimenti di Eccellenza – 2018–2022). L.B. wishes to thank funding from the European Union, Next Generation EU, AdP POR project L.A. 1.1.35 CUP: B93C22000630006. Open Access funding provided by Università degli Studi di Perugia within the CRUI-CARE Agreement.

Conflict of Interest

The authors declare no conflict of interest.

Data Availability Statement

The data that support the findings of this study are available in the supplementary material of this article.

Keywords: computational chemistry · gold-aluminyl complexes · catalysis · reaction mechanisms · small-molecule activation

[1] J. Hicks, A. Mansikkamäki, P. Vasko, J. M. Goicoechea, S. Aldridge, *Nat. Chem.* **2019**, *11*, 237–241.
[2] D. Sorbelli, L. Belpassi, P. Belanzoni, *J. Am. Chem. Soc.* **2021**, *143*, 14433–14437.
[3] D. Sorbelli, L. Belpassi, P. Belanzoni, *Inorg. Chem.* **2022**, *61*, 1704–1716.
[4] D. Sorbelli, E. Rossi, R. W. A. Havenith, J. E. M. N. Klein, L. Belpassi, P. Belanzoni, *Inorg. Chem.* **2022**, *61*, 7327–7337.
[5] D. Sorbelli, L. Belpassi, P. Belanzoni, *Chem. Sci.* **2022**, *13*, 4623–4634.
[6] I. F. Leach, D. Sorbelli, L. Belpassi, P. Belanzoni, R. W. A. Havenith, J. E. M. N. Klein, *Dalton Trans.* **2023**, *52*, 11–15.
[7] D. Sorbelli, L. Belpassi, P. Belanzoni, *Inorg. Chem.* **2022**, *61*, 21095–21106.
[8] F. Hanusch, L. Groll, S. Inoue, *Chem. Sci.* **2021**, *12*, 2001–2015.
[9] J. Li, M. Hermann, G. Frenking, C. Jones, *Angew. Chem. Int. Ed.* **2012**, *51*, 8611–8614; *Angew. Chem.* **2012**, *124*, 8739–8742.
[10] G. H. Spikes, J. C. Fettinger, P. P. Power, *J. Am. Chem. Soc.* **2005**, *127*, 12232–12233.
[11] J. Li, C. Schenk, C. Goedecke, G. Frenking, C. Jones, *J. Am. Chem. Soc.* **2011**, *133*, 18622–18625.
[12] T. J. Hadlington, M. Hermann, J. Li, G. Frenking, C. Jones, *Angew. Chem. Int. Ed.* **2013**, *52*, 10199–10203; *Angew. Chem.* **2013**, *125*, 10389–10393.
[13] M. Hermann, C. Goedecke, C. Jones, G. Frenking, *Organometallics* **2013**, *32*, 6666–6673.
[14] D. Sorbelli, L. Belpassi, P. Belanzoni, *Chem. Sci.* **2023**, *14*, 889–896.
[15] Y. Peng, M. Brynda, B. D. Ellis, J. C. Fettinger, E. Rivard, P. P. Power, *Chem. Commun.* **2008**, 6042–6044.
[16] T. J. Hadlington, J. Li, M. Hermann, A. Davey, G. Frenking, C. Jones, *Organometallics* **2015**, *34*, 3175–3185.
[17] L. Zhao, C. Jones, G. Frenking, *Chem. Eur. J.* **2015**, *21*, 12405–12413.
[18] C. McManus, A. E. Crumpton, S. Aldridge, *Chem. Commun.* **2022**, *58*, 8274–8277.
[19] D. Wendel, T. Szilvási, D. Henschel, P. J. Altmann, C. Jandl, S. Inoue, B. Rieger, *Angew. Chem. Int. Ed.* **2018**, *57*, 14575–14579; *Angew. Chem.* **2018**, *130*, 14783–14787.
[20] C. McManus, J. Hicks, X. Cui, L. Zhao, G. Frenking, J. M. Goicoechea, S. Aldridge, *Chem. Sci.* **2021**, *12*, 13458–13468.
[21] H. Y. Liu, S. E. Neale, M. S. Hill, M. F. Mahon, C. L. McMullin, *Dalton Trans.* **2022**, *51*, 3913–3924.
[22] M. Navarro, J. J. Moreno, M. Pérez-Jiménez, J. Campos, *Chem. Commun.* **2022**, *58*, 11220.
[23] J. Campos, *Nat. Chem. Rev.* **2020**, *4*, 696–702.
[24] D. G. H. Hetterscheid, J. I. Van Der Vlugt, B. De Bruin, J. N. H. Reek, *Angew. Chem. Int. Ed.* **2009**, *48*, 8178–8181; *Angew. Chem.* **2009**, *121*, 8324–8327.
[25] H. Dau, C. Limberg, T. Reier, M. Risch, S. Roggan, P. Strasser, *ChemCatChem* **2010**, *2*, 724–761.
[26] T. Jafari, E. Moharreri, A. S. Amin, R. Miao, W. Song, S. L. Suib, *Molecules* **2016**, *21*, 900.
[27] P. Preuster, C. Papp, P. Wasserscheid, *Acc. Chem. Res.* **2017**, *50*, 74–85.
[28] S. Luo, H. Lin, Q. Wang, X. Ren, D. Hernández-Pinilla, T. Nagao, Y. Xie, G. Yang, S. Li, H. Song, M. Oshikiri, J. Ye, *J. Am. Chem. Soc.* **2021**, *143*, 12145–12153.
[29] J. I. Van der Vlugt, *Chem. Soc. Rev.* **2010**, *39*, 2302–2322.
[30] S. Streiff, F. Jérôme, *Chem. Soc. Rev.* **2021**, *50*, 1512–1521.
[31] G. Kovács, A. Lledós, G. Ujaque, *Angew. Chem. Int. Ed.* **2011**, *50*, 11147–11151; *Angew. Chem.* **2011**, *123*, 11343–11347.
[32] A. Robock, L. Oman, G. L. Stenchikov, *J. Geophys. Res. [Atmos.]* **2008**, *113*, 16101.
[33] T. Y. Chiang, T. H. Yuan, R. H. Shie, C. F. Chen, C. C. Chan, *Environ. Int.* **2016**, *96*, 1–7.
[34] Q. Zhong, H. Shen, X. Yun, Y. Chen, Y. Ren, H. Xu, G. Shen, W. Du, J. Meng, W. Li, J. Ma, S. Tao, *Environ. Sci. Technol.* **2020**, *54*, 6508–6517.
[35] Y. Wang, Z. Yao, Z. Pan, E. A. Davidson, D. Kanter, *Environ. Res. Lett.* **2014**, *9*, 105012.
[36] A. R. Ravishankara, J. S. Daniel, R. W. Portmann, *Science* **2009**, *326*, 123–125.
[37] M. J. Prather, *Science* **1998**, *279*, 1339–1341.
[38] D. J. Wuebbles, *Science* **2009**, *326*, 56–57.
[39] W. G. Zumft, P. M. H. Kroneck, *Adv. Microb. Physiol.* **2006**, *52*, 107–227.
[40] A. Pomowski, W. G. Zumft, P. M. H. Kroneck, O. Einsle, *Natur* **2011**, *477*, 234–237.
[41] L. Zhang, A. Wüst, B. Prasser, C. Müller, O. Einsle, *Proc. Natl. Acad. Sci. USA* **2019**, *116*, 12822–12827.
[42] F. Le Vaillant, A. Mateos Calbet, S. González-Pelayo, E. J. Reijerse, S. Ni, J. Busch, J. Cornella, *Natur* **2022**, *604*, 677–683.
[43] K. Severin, *Chem. Soc. Rev.* **2015**, *44*, 6375–6386.
[44] S. Sinhababu, Y. Lakliang, N. P. Mankad, *Dalton Trans.* **2022**, *51*, 6129–6147.
[45] I. Fernández, F. M. Bickelhaupt, *Chem. Soc. Rev.* **2014**, *43*, 4953–4967.
[46] F. M. Bickelhaupt, K. N. Houk, *Angew. Chem. Int. Ed.* **2017**, *56*, 10070–10086; *Angew. Chem.* **2017**, *129*, 10204–10221.
[47] P. Vermeeren, S. C. C. van der Lubbe, C. Fonseca Guerra, F. M. Bickelhaupt, T. A. Hamlin, *Nat. Protoc.* **2020**, *15*, 649–667.
[48] K. Morokuma, *J. Chem. Phys.* **1971**, *55*, 1236–1244.
[49] T. Ziegler, A. Rauk, *Theor. Chim. Acta* **1977**, *46*, 1–10.
[50] L. Zhao, M. von Hopffgarten, D. M. Andrada, G. Frenking, *Wiley Interdiscip. Rev.: Comput. Mol. Sci.* **2018**, *8*, 1345.
[51] L. Belpassi, I. Infante, F. Tarantelli, L. Visscher, *J. Am. Chem. Soc.* **2008**, *130*, 1048–1060.
[52] G. Bistoni, S. Rampino, F. Tarantelli, L. Belpassi, *J. Chem. Phys.* **2015**, *142*, 084112.
[53] "GitHub – BERTHA-4c-DKS/pycubescd," can be found under https://github.com/BERTHA-4c-DKS/pycubescd, **n.d**.
[54] M. Mitoraj, A. Michalak, *J. Mol. Model.* **2007**, *13*, 347–355.
[55] S. Sinhababu, M. R. Radzhabov, J. Telser, N. P. Mankad, *J. Am. Chem. Soc.* **2022**, *144*, 3210–3221.
[56] W. B. Tolman, *Angew. Chem. Int. Ed.* **2010**, *49*, 1018–1024; *Angew. Chem.* **2010**, *122*, 1034–1041.
[57] P. Chen, S. I. Gorelsky, S. Ghosh, E. I. Solomon, *Angew. Chem. Int. Ed.* **2004**, *43*, 4132–4140; *Angew. Chem.* **2004**, *116*, 4224–4233.
[58] S. I. Gorelsky, S. Ghosh, E. I. Solomon, *J. Am. Chem. Soc.* **2006**, *128*, 278–290.
[59] I. Bar-Nahum, A. K. Gupta, S. M. Huber, M. Z. Ertem, C. J. Cramer, W. B. Tolman, *J. Am. Chem. Soc.* **2009**, *131*, 2812–2814.
[60] L. M. Aguirre Quintana, Y. Yang, A. Ramanathan, N. Jiang, J. Bacsa, L. Maron, H. S. La Pierre, *Chem. Commun.* **2021**, *57*, 6664–6667.
[61] X. Chen, H. Wang, S. Du, M. Driess, Z. Mo, *Angew. Chem. Int. Ed.* **2022**, *61*, e202114598.

[62] Y. Pang, M. Leutzsch, N. Nöthling, J. Cornella, *J. Am. Chem. Soc.* **2020**, *142*, 19473–19479.
[63] H. W. Moon, J. Cornella, *ACS Catal.* **2022**, *12*, 1382–1393.
[64] X. Li, X. Liu, P. Sun, Y. Feng, H. Shan, X. Wu, J. Xu, C. Huang, Z. K. Chen, Z. X. Xu, *RSC Adv.* **2017**, *7*, 17076–17084.
[65] M. Ito, M. Itazaki, H. Nakazawa, *J. Am. Chem. Soc.* **2014**, *136*, 6183–6186.
[66] G. te Velde, F. M. Bickelhaupt, E. J. Baerends, C. Fonseca Guerra, S. J. A. van Gisbergen, J. G. Snijders, T. Ziegler, *J. Comput. Chem.* **2001**, *22*, 931–967.
[67] *ADF Manual ADF Program System Release 2014*, **1993**.
[68] M. Swart, F. M. Bickelhaupt, *J. Comput. Chem.* **2008**, *29*, 724–734.
[69] J. P. Perdew, K. Burke, M. Ernzerhof, *Phys. Rev. Lett.* **1996**, *77*, 3865–3868.
[70] E. Van Lenthe, E. J. Baerends, J. G. Snijders, *J. Chem. Phys.* **1993**, *99*, 4597–4610.
[71] E. Van Lenthe, E. J. Baerends, J. G. Snijders, *J. Chem. Phys.* **1994**, *101*, 9783–9792.
[72] E. Van Lenthe, *J. Chem. Phys.* **1999**, *110*, 8943–8953.
[73] S. Grimme, J. Antony, S. Ehrlich, H. Krieg, *J. Chem. Phys.* **2010**, *132*, 154104.
[74] S. Grimme, S. Ehrlich, L. Goerigk, *J. Comput. Chem.* **2011**, *32*, 1456–1465.
[75] C. C. Pye, T. Ziegler, *Theor. Chem. Acc.* **1999**, *101*, 396–408.
[76] D. Sorbelli, P. Belanzoni, L. Belpassi, J. W. Lee, G. Ciancaleoni, *J. Comput. Chem.* **2022**, *43*, 717–727.
[77] D. H. Ess, S. E. Wheeler, R. G. Iafe, L. Xu, N. Çelebi-Ölçüm, K. N. Houk, *Angew. Chem. Int. Ed.* **2008**, *47*, 7592–7601; *Angew. Chem.* **2008**, *120*, 7704–7713.

Manuscript received: November 17, 2022
Accepted manuscript online: January 20, 2023
Version of record online: March 9, 2023